Chemistry & Biology
Article

Toward the Rational Design of p53-Stabilizing Drugs: Probing the Surface of the Oncogenic Y220C Mutant

Nicolas Basse,[1,2] Joel L. Kaar,[1,2] Giovanni Settanni,[1] Andreas C. Joerger,[1] Trevor J. Rutherford,[1] and Alan R. Fersht[1,*]
[1]Medical Research Council Centre for Protein Engineering, Cambridge, CB2 0QH, UK
[2]These authors contributed equally to this work
*Correspondence: arf25@cam.ac.uk
DOI 10.1016/j.chembiol.2009.12.011

SUMMARY

The p53 cancer mutation Y220C induces formation of a cavity on the protein's surface that can accommodate stabilizing small molecules. We combined fragment screening and molecular dynamics to assess the druggability of p53-Y220C and map ligand interaction sites within the mutational cavity. Elucidation of the binding mode of fragment hits by crystallography yielded a clear picture of how a drug might dock in the cavity. Simulations that solvate the protein with isopropanol found additional sites that extend the druggable surface. Moreover, structural observations and simulation revealed the dynamic landscape of the cavity, which improves our understanding of the impact of the mutation on p53 stability. This underpins the importance of considering flexibility of the cavity in screening for optimized ligands. Our findings provide a blueprint for the design of effective drugs that rescue p53-Y220C.

INTRODUCTION

Mutation of the tumor suppressor p53, an essential mediator of cellular response to oncogenic stresses, is the most frequent genetic alteration in human cancer (Hann and Lane, 1995; Hollstein et al., 1991; Levine et al., 1991; Vousden and Lane, 2007). Approximately 30% of the mutations that inactivate p53 simply lower the melting temperature (T_m) of the core DNA-binding domain of p53 (Bullock et al., 1997; Bullock et al., 2000) so that it denatures rapidly in cells (Friedler et al., 2003). In theory, the T_m of such a mutant, and hence its activity, can be restored by molecules that selectively bind to its native structure and not its denatured states (Bullock and Fersht, 2001; Joerger and Fersht, 2007). Functional studies in cells that show temperature-sensitive mutants of p53 are transcriptionally active at low temperatures (<37°C) provide evidence that the activity of such mutants can be rescued in a biological context (Di Como and Prives, 1998).

The principle of p53 reactivation by small molecules was first demonstrated using a small peptide, CDB3, which binds reversibly to the DNA-binding domain of p53. The peptide was shown to stabilize wild-type and mutant p53 in vitro (Friedler et al., 2002) and elevated the activity of mutant p53 in cancer cell lines (Issaeva et al., 2003). There have been numerous reports of other molecules that restore mutant p53 activity in cells (Bykov et al., 2002; Bykov et al., 2005; Foster et al., 1999; North et al., 2002). However, how these molecules reactivate p53 or, in the case of those that are known not to bind wild-type or mutant p53 (i.e., CP-31398), induce p53-like effects remains uncertain. It has recently been proposed that a select group of molecules (i.e., PRIMA-1 and MIRA-1) or their respective hydrolysis products may react covalently with p53 via modification of cysteine residues, suggesting a possible mechanism for targeting p53 in cells (Lambert et al., 2009). It is plausible that molecules that bind to cysteine residues in p53 may also regulate p53 activity through modulation of the protein's redox state. Given the ramifications toward the development of novel anticancer drugs, there is a fundamental need to discover small molecules that directly stabilize temperature-sensitive p53 mutants.

The Y220C mutation, one of the more prevalent oncogenic mutations in p53 (associated with ~75,000 new cancer cases per annum; Joerger and Fersht, 2008; Petitjean et al., 2007), presents an almost ideal paradigm for searching for and studying small molecules that stabilize p53 in a mutation-specific way. Mutation of the tyrosine to a cysteine markedly lowers the thermodynamic stability of the protein and, notably, induces formation of a potentially druggable cavity on the protein's surface at the mutation site, which is distant from the functional surface region of the protein, without otherwise perturbing its overall structure (Joerger et al., 2006). Hence, a small molecule could be targeted to the mutational cavity, with the presumption that binding, while stabilizing the protein, would not affect the function of p53. Furthermore, such a molecule would not bind to wild-type p53 in noncancerous cells.

We recently reported the discovery of PhiKan083, a carbazole derivative that binds to the mutational cavity of p53-Y220C, using a simple in silico docking algorithm (Boeckler et al., 2008). The molecule, which binds with moderate affinity (K_d ~150 μM) and also raises the T_m and slows down the rate of denaturation of p53-Y220C, is the first such lead for mutant-specific p53 drugs. A notable outcome of this work was that small induced-fit movements in the protein could have large effects on in silico predictions, which can affect the nature of the resulting hits. This finding underpins the need for complementary methods of searching for molecules that bind

p53-Y220C and ascertaining the druggable properties of the binding site.

Here, we describe the use of fragment screening and molecular dynamics (MD) simulations to further explore the druggable surface of the p53-Y220C mutant. Specifically, we attempted to identify all possible ligand interaction sites (i.e., "hot spots") on the surface of the mutational cavity, which, collectively, provide a blueprint for the design of molecules that bind to p53-Y220C with druglike (submicromolar) affinity. We also sought novel lead scaffolds with unique binding modes that expand our present picture of how a drug could dock within the cavity. Together, the identification of ligand binding hotspots and novel scaffolds present the necessary basis for optimizing PhiKan083 as well as alternative starting points for drug design.

Fragment-based ligand screening has emerged as a powerful tool for assessing the druggability of proteins and ascertaining sites that interact with ligands (Bembenek et al., 2009; Ciulli and Abell, 2007; Hajduk and Greer, 2007; Hajduk et al., 2005b). This technique entails the use of molecules of low molecular weight and chemical complexity to probe for areas that are energetically favorable for ligand binding. The propensity of fragment molecules to interact with a protein is indicative of whether a protein can accommodate a molecule with druglike properties (Hajduk et al., 2005a). Similarly, computational and experimental methods that use organic solvents as probes can be used to map ligand-binding sites on proteins (Dennis et al., 2002; Liepinsh and Otting, 1997; Seco et al., 2009).

In this work, we have screened the core domain of p53-Y220C against a fragment library by water-ligand-observed-gradient spectroscopy (waterLOGSY) and thermal denaturation scanning fluorimetry. Fragment binding was subsequently confirmed by heteronuclear single-quantum coherence ($^{15}N/^{1}H$ HSQC) NMR. The binding mode of several fragments was solved by X-ray crystallography. Moreover, MD simulations have been used to probe the dynamic properties of the mutational cavity and the preferential binding modes of isopropanol, which mimics a small-molecule drug.

RESULTS AND DISCUSSION

Fragment Screening

Ligand-binding sites on T-p53C-Y220C, a stable variant of p53 core domain (Joerger et al., 2004; Nikolova et al., 1998) with the Y220C mutation, were initially explored by screening against a chemically diverse fragment library. The library of nearly 1900 molecules was designed according to the generalized rule-of-three for the physicochemical properties of fragments (Congreve et al., 2003). To minimize the number of false-positive and false-negative results (fragments that bind T-p53C-Y220C but are not detected), two parallel methods including waterLOGSY, a one-dimensional ligand-observed NMR method, and thermal denaturation scanning fluorimetry, which scans the effect of a ligand on the T_m of a protein using an exogenous fluorescent dye, were used for screening.

Screening by waterLOGSY and thermal denaturation scanning fluorimetry found 205 and 47 fragment hits against T-p53C-Y220C, respectively (Table 1). Of the hits identified by thermal denaturation scanning fluorimetry, the maximum observed shift in T_m was 1.8 ± 0.2°C. Binding of the fragment hits from both methods was subsequently confirmed by $^{15}N/^{1}H$ HSQC, which is widely considered the most definitive assay for detecting protein-ligand binding interactions (Hajduk et al., 2005b). The final hit rates for waterLOGSY and thermal denaturation scanning fluorimetry, considering only the fragments for which binding was confirmed, were 3.7% and 0.9%, respectively. Comparison of the hit rates indicates that a large number of fragment hits were missed by thermal denaturation scanning fluorimetry. A likely cause of false-negative results in this assay is fluorescence quenching by the fragment molecules. Additionally, analysis of the hit rate provides an estimate of the druggability of T-p53C-Y220C, as suggested by Hajduk et al. (2005a). The combined hit rate is only marginally lower than the reported threshold value for proteins for which high-affinity ligands have been developed.

Table 1. Results of Fragment Screening of T-p53C-Y220C by WaterLOGSY and Thermal Denaturation Scanning Fluorimetry

Variable	WaterLOGSY	Thermal Denaturation Scanning Fluorimetry
No. of fragments screened	1895	1895
No. of identified hits	205	47
No. of hits confirmed by $^{15}N/^{1}H$ HSQC	70	17
Final hit ratio, %[a]	3.7	0.9

[a] Hit ratio is defined as the ratio of the number of identified or confirmed hits to the total number of fragments screened.

Analysis of the final fragment hits, of which there were 84 in total, found a number of structural similarities. These similarities constitute pharmacophore features that can be used to classify the fragment hits. The fragments could be classified in seven unique families, as shown in Figure 1. Among the key pharmacophore features that differentiate the families are the number of rings in the central scaffold as well as the spacing between rings when there is more than one, aromaticity of the ring system, number of molecules in each ring, and the size of attached substituent groups. Molecule 14 was found to have the tightest binding affinity (K_d = 105 ± 12 μM) of the confirmed hits. Although it is difficult to predict the implications of the distinctive structural features with respect to possible interactions formed between the fragments and protein, it is highly likely that the ring system of the respective fragments mimics the side chain of the mutated tyrosine, packing between the hydrophobic residues that line the cavity (Joerger et al., 2006).

Thermal denaturation scanning fluorimetry represents a relatively new biophysical technique for fragment screening (Ciulli and Abell, 2007). Despite growing interest in this technique for screening, there is little data on its utility in measuring weak binding affinities, which are characteristic of fragments. To the best of our knowledge, this report is the first direct comparison of thermal denaturation scanning fluorimetry and NMR, a conventional tool for assaying ligands with a broad range of binding affinities, for fragment screening. Of the confirmed hits, 17 were found from thermal denaturation scanning fluorimetry and 70 from waterLOGSY. Interestingly, only three of the hits were identified in both assays, indicating that the overlap of hits from the respective methods was low. These fragments do not share any obvious structural similarities from which conclusions can be drawn about why they were identified in both assays or,

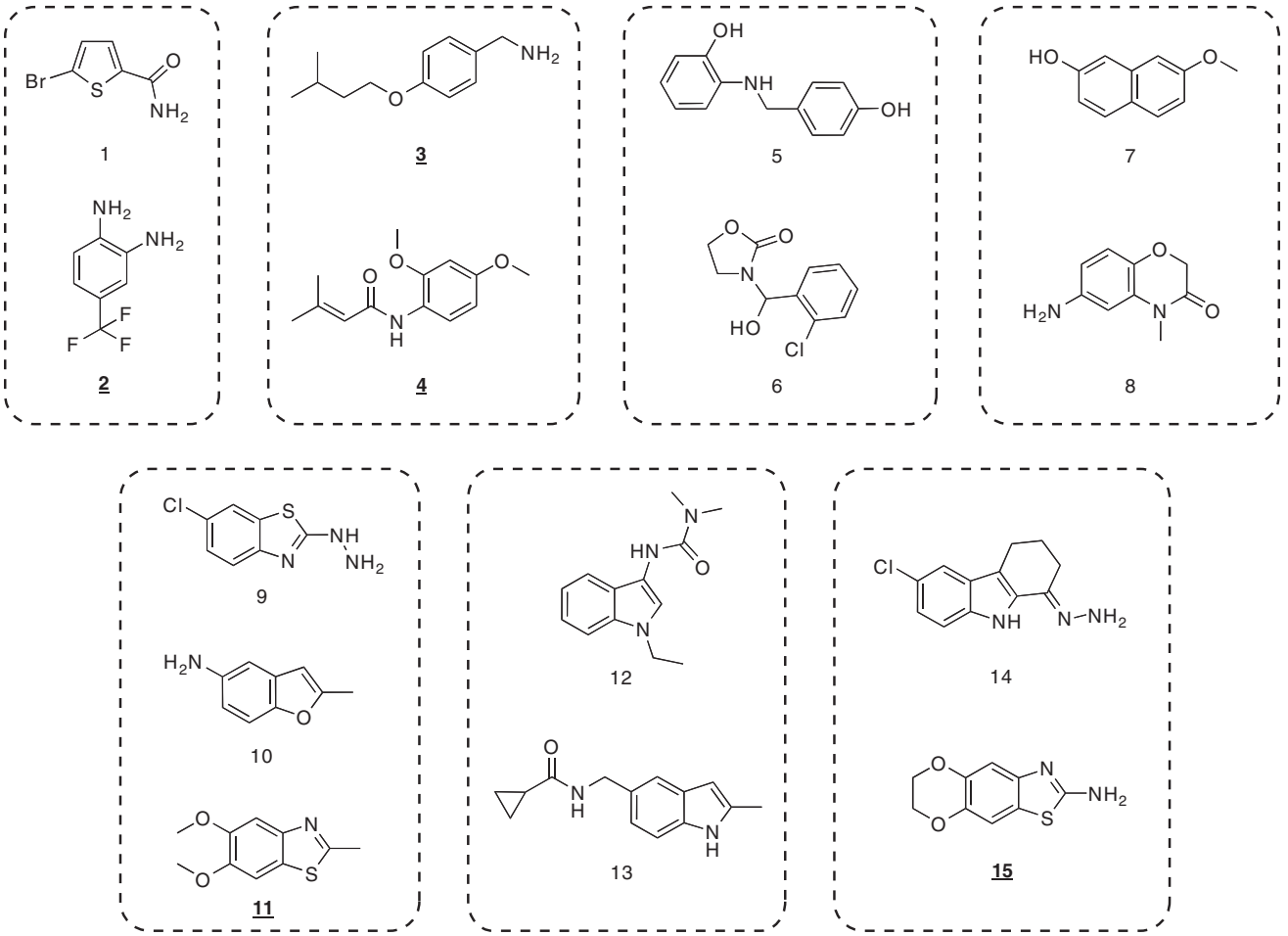

Figure 1. Pharmacophore Classification of Confirmed Fragments Hits

The fragment hits were classified on the basis of chemical structure. Representative structures of each classification are presented and separated accordingly. The fragment hits whose binding modes to T-p53C-Y220C were solved via X-ray crystallography are indicated in bold and underlined.

more importantly, why binding of the fragments was not detected in both assays. The screening results clearly show that, although thermal denaturation scanning fluorimetry is not as sensitive as waterLOGSY (i.e., has a higher rate of false negatives), it can potentially still generate unique hits and thus can be useful as a complementary fragment screening technique.

Identification of Target Binding Site of Fragment Hits

Analysis of ligand binding by $^{15}N/^{1}H$ HSQC provides site-specific resolution of the binding surface on the protein. The target binding site can be inferred from mapping chemical shifts in resonances of residues that are perturbed upon binding (Meyer and Peters, 2003). Because T-p53C-Y220C is a highly destabilized protein, only a partial resonance assignment was obtainable from analogy with wild-type p53, where peaks overlaid, and limited triple resonance NMR data of the mutant protein. Unfortunately, resonances close to the mutation site differ significantly from those in the spectra of wild-type, and these were most difficult to assign with the required certainty.

Qualitative analysis of chemical shifts in $^{15}N/^{1}H$ HSQC spectra of T-p53C-Y220C in complex with the fragment hits found multiple peak perturbations (Figure 2). Residues Val147 and Asp148, both of which are positioned in the central region of the cavity, are among those clearly disturbed by each of the confirmed fragment hits (Figure 2; lower panels). In the spectra for many of the fragment hits, residues Tyr107, Thr155, and Ser260, all of which are also in the cavity region, are also shifted. Perturbations of these residues, coupled with the observation that assigned residues outside the cavity are unaffected by binding, implies that the fragments bind exclusively to the cavity region. A number of other prominent shifts in peaks that were not assigned, but thought to be of residues in the cavity region, further support the conclusion that the fragments bind to the mutation site. Because of the absence of disturbances at other sites on the protein, it can be further inferred that wild-type p53 is a very challenging target, consistent with structural observations showing it lacks pronounced surface crevices and that only p53 mutants with altered surface properties (but unperturbed DNA-contact surfaces) are candidate drug targets. Consistent with this, a screen of wild-type p53 core domain (T-p53C) by waterLOGSY and thermal denaturation scanning fluorimetry did not find any fragment hits. Additionally,

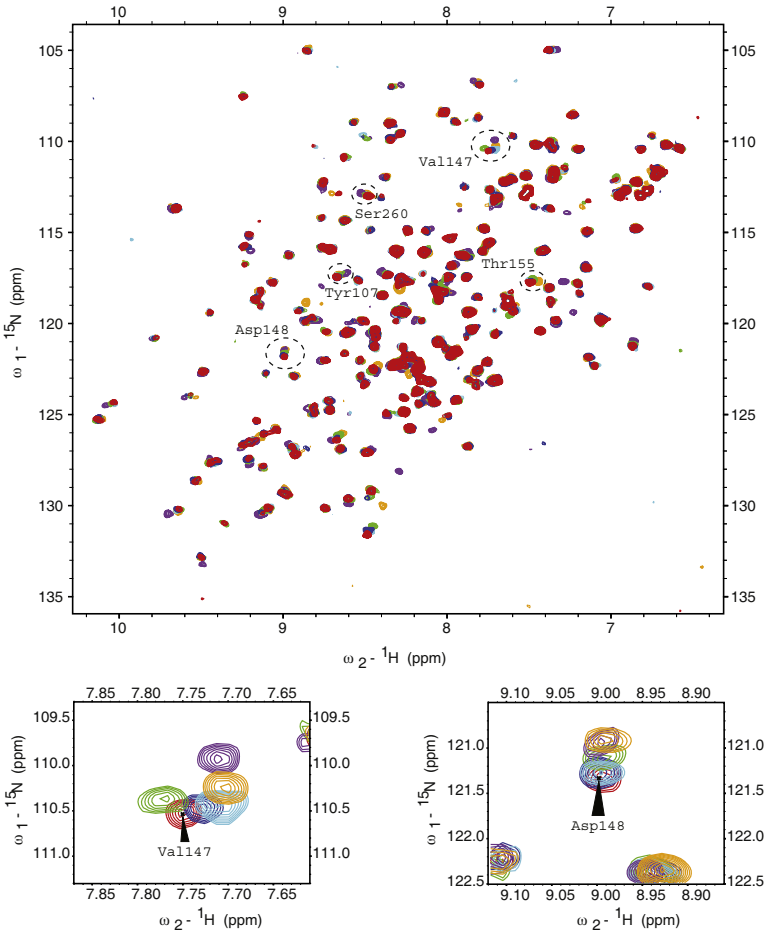

Figure 2. Overlay of $^{15}N/^{1}H$ HSQC Spectra of T-p53C-Y220C

Shown are T-p53C-Y220C alone (red) and T-p53C-Y220C in the presence of fragments 2 (1 mM; blue), 3 (1 mM; cyan), 4 (1 mM; orange), 11 (1 mM; green), and 15 (1 mM; purple). Resonances for residues Val147, Asp148, Tyr107, Thr155, and Ser260, which are in or near the mutational cavity, are indicated. The lower panels show magnified views of spectral changes to residues Val147 and Asp148 upon addition of the fragments.

noticeable differences in shifts in a small number of resonance peaks between spectra suggest the fragments may bind with different binding modes. However, the exact positioning and overall orientation of the molecules in the binding pocket cannot be determined from analysis of $^{15}N/^{1}H$ HSQC data alone and requires the use of structure determination methods.

Structural Determination of Fragment-Binding Modes

In an attempt to elucidate the binding mode of all confirmed fragment hits, crystals of T-p53C-Y220C were soaked with the individual fragments and structures of the resulting protein-ligand complex determined by X-ray crystallography. Because of low occupancy of the fragments within the cavity and disruption of the crystal packing upon fragment binding, structural elucidation of the binding mode was possible only for a small subset of the confirmed fragments hits (Figure 1). The resolution of the solved complex structures was in the range of 1.6–2.1 Å (see Table 2 for data collection and refinement statistics). An electron density map for fragment 15 is shown in Figure S1 available online. In all structures, the small molecule occupied only one of the two molecules in the asymmetric unit (chain B), which is consistent with our earlier data (Boeckler et al., 2008).

The general binding mode of fragments 2, 11, and 15 involves sandwiching of the ring systems between Pro151 and Val147 on one side of the cavity and Pro222 and Pro223 on the other (Figures 3A–3C). As a result of binding, the sulfhydryl group of the mutated Cys220 residue at the bottom of the cavity is displaced, thus deepening the pocket by ~2 Å and, in turn, allowing accommodation of the ligands. This flip of the cysteine side chain triggers a concerted movement in two hydrophobic side chains (Val157 and Ile232) in the interior of the protein. Additionally, shifts in a number of residues around the periphery of the cavity (e.g., Thr150 and Pro222) are observed upon binding, which are indicative of the flexibility of the cavity.

The structure of fragment 15 bound to T-p53C-Y220C (solved at 1.6 Å resolution) shows that the molecule sits deeply within the mutation-induced cavity (Figure 3A). The sulfur atom on the thiazole ring is positioned near the mutated Cys220 residue at the deepest part of the cleft. In addition to hydrophobic packing interactions, fragment 15 forms specific hydrogen bonds with the protein and water molecules. Most significantly, the substituent amine in the 2-position on the thiazole ring makes a hydrogen bond with the carbonyl oxygen of Leu145 and a conserved water molecule that bridges the amine with the main chain of Asp228. As such, it occupies the position of a water molecule in the ligand-free structure that is displaced upon binding. The thiazole nitrogen and oxygen of the dioxane ring are also involved in water-mediated hydrogen bonds.

Fragment 11, which also contains an aromatic benzothiazole ring system, binds in the same plane as fragment 15 within the cavity but sits in a more upright position (Figure 3B). Positioned as such, the thiazole nitrogen is within hydrogen-bonding distance of the hydroxyl group of Thr150. The methoxy moieties of the molecule sit at the bottom of the cavity in close proximity to Cys220.

The binding mode of fragment 2 (determined at 1.8 Å resolution) is unique in that two molecules are bound within the cavity (Figure 3C). The molecules are positioned at opposite sides of the cavity with the trifluoromethyl groups of each pointing toward the mutated Cys220 residue. Binding of molecule *a* is stabilized by the interaction of the amine at position 2 on the aromatic ring with the carbonyl oxygen of Leu145 and a conserved water molecule, thus mimicking the binding mode of the amino group in fragment 15. The amines at positions 1 and 2 are both involved in a network of hydrogen-bond interactions with water molecules. Molecule *a* makes hydrophobic interactions with Val147

Table 2. Data Collection and Refinement Statistics for T-p53C-Y220C Ligand Structures

Variable	Fragment 15	Fragment 11	Fragment 2
Data collection			
Space group	$P2_12_12_1$	$P2_12_12_1$	$P2_12_12_1$
Cell, *a, b, c*, Å	65.06, 71.14, 105.41	65.25, 70.58, 105.44	65.23, 71.09, 105.39
Molecules/ASU	2	2	2
Resolution, Å[a]	35.5–1.60 (1.69–1.60)	35.5–2.10 (2.21–2.10)	41.1–1.80 (1.90–1.80)
Unique reflections	65,261	29,108	45,419
Completeness, %[a]	99.9 (100)	99.9 (100)	98.7 (97.9)
Multiplicity [a]	6.2 (5.8)	3.5 (3.6)	3.7 (3.7)
R_{merge}, %[a,b]	7.0 (31.1)	10.8 (29.4)	6.3 (22.4)
$< I/\sigma_I >$[a]	15.8 (5.2)	8.6 (4.1)	14.2 (5.5)
Wilson *B* value, Å^2	13.8	15.4	14.0
Refinement			
No. of atoms			
Protein[c]	3105	3080	3089
Water	656	523	601
Ligand	14	14	24
Zinc	2	2	2
R_{cryst}, %[d]	16.5	17.2	15.9
R_{free}, %[d]	19.3	22.8	19.0
Rmsd bonds, Å	0.007	0.007	0.008
Rmsd angles, °	1.12	1.0	1.14
Mean *B* value, Å^2	17.3	16.6	17.1
Ramachandran statistics[e]			
Allowed/favored, %	100/99.5	100/99.0	100/99.5

[a] Data in parentheses are for the highest resolution shell.
[b] $R_{merge} = \sum(I_{h,i} - < I_h >)/\sum I_{h,i}$.
[c] Number includes alternative conformations.
[d] R_{cryst} and $R_{free} = \sum||F_{obs}| - |F_{calc}||/\sum|F_{obs}|$ where R_{free} was calculated over 5% of the amplitudes chosen at random and not used in the refinement.
[e] Calculated with MOLPROBITY (Davis et al., 2007).

and Pro222, partially overlapping with the positioning of the fragments 15 and 11, whereas molecule *b* packs between the hydrophobic side chains of Pro153 and Pro222 at a site that is not occupied by the other fragments. The fluorine atoms likely play a significant role in binding by coordinating strongly with the protein. Moreover, the fluorine atoms can indirectly strengthen the binding interaction of the fragment by polarizing the amine groups attached to the benzene ring. The fluorination of leadlike molecules can markedly enhance their binding affinity and overall biological activity (Bohm et al., 2004).

Structures of T-p53C-Y220C in complex with fragments 3 and 4 were also solved; however, only partial electron density for the fragments was observed (data not shown). Consequently, the exact binding mode of the fragments within the cavity could not be unambiguously modeled. The parts of the fragments that showed the clearest density were the aromatic rings, which were positioned between Pro151 and Pro222, suggesting their binding modes were similar to that of fragments 2, 11, and 15.

MD Simulations of T-p53C-Y220C Solvation by Isopropanol

Seco et al. (2009) previously demonstrated the possibility to identify drug-binding sites and protein-protein interaction interfaces on proteins of pharmacological interest using MD simulations of proteins in mixtures of water and isopropanol. Similarly, Guvench and MacKerell (2009) used MD simulations of the protein BCL-6 in solutions of organic solvents in water to map the affinity of hydrophobic and aromatic molecules on the protein's surface. Using the simulation results, the authors were able to accurately predict the binding mode of two peptide substrates, which was confirmed by X-ray crystallography. To explore further the druggable surface of T-p53C-Y220C, we determined the preferential solvation of the protein by MD simulation with isopropanol (20% v/v). In the simulation, isopropanol represents a theoretical ligand with polar and nonpolar properties that can bind to T-p53C-Y220C via hydrogen bonding and hydrophobic interactions.

Over the time course of the simulation, the MD trajectory of T-p53C-Y220C remained close to the x-ray structure (backbone RMSD ~1.5 Å). Analysis of the resulting isopropanol density isosurface of T-p53C-Y220C found several regions of high density of isopropanol. The area of highest density of isopropanol was found on the surface that forms the self-complementary core domain-core domain interface upon binding to a DNA half-site (Kitayner et al., 2006) and a surface patch around Leu188 and Leu201. However, because only the site of the mutation proved

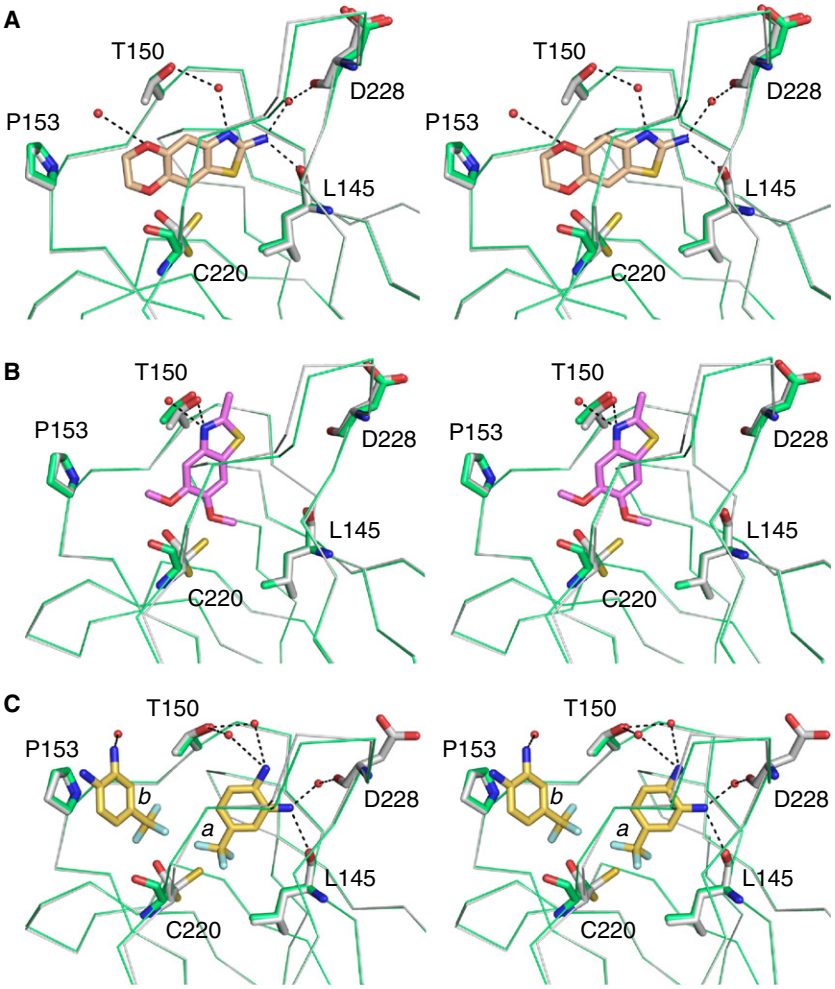

Figure 3. Binding Mode of Lead Fragments in the Mutation-Induced Cavity of T-p53C-Y220C

(A–C) Stereo view of the Y220C cavity with bound fragments 15 (A), 11 (B), and 2 (C) is shown. In all three cases, the fragment-bound structure (green) is superimposed onto the structure of the ligand-free mutant (PDB code 2J1X; gray). Polar contacts of fragments with the protein and water molecules (red spheres) are shown as dashed lines.

to bind small molecules, as was evident by the fragment screening, we focused our analysis solely on this site.

The density of isopropanol in the mutation-induced cavity was more than four times higher than the expected value for the bulk mixture, indicating the propensity of solvent binding in the pocket. Localization of isopropanol molecules within the cavity between Pro153, Pro222, and Cys220 was observed (Figure 4A). The hydroxyl group of isopropanol made hydrogen bonds with the backbone carbonyl oxygen of Pro151 and Pro152. The estimated binding free energy associated with the interaction of isopropanol at this site is −3.9 kcal/mol, as calculated with the procedure proposed by Seco et al. (2009). Conversely, the area of the cavity between the side chains of Val147, Pro151, and Pro223, corresponding to the area occupied by the aromatic ring system of the bound fragments, was devoid of isopropanol molecules. The absence of isopropanol in this area can presumably be attributed to the available space of the cavity, which cannot accommodate isopropanol molecules in an energetically favorable configuration. Importantly, differences in the chemical nature of isopropanol and the cyclic fragment molecules allowed us to explore distinctly different binding sites using isopropanol as a molecular probe.

In addition to yielding solvation patterns of isopropanol on T-p53C-Y220C, the MD simulation illuminates how structural motions in the cavity may affect ligand binding. Analysis of the cavity dynamics found that the width of the region where isopropanol binds is highly flexible. Fluctuations in the side chain of Pro222, in particular, greatly altered the cavity width. The distance between the C_α of Pro153 and the C_γ of Pro222 ranged from 5-9 Å over the time-course of the simulation (Figure 4B). During the initial 3 ns, when isopropanol molecules occupy the cavity, the cavity width at this point varied between 7 Å and 9 Å, which matches that observed in the crystal structures of the free and fragment-bound protein. In the absence of isopropanol, the cavity fluctuated between an apparent open and closed state, where the distance between the defined points was 5–7 Å. Dynamic fluctuations in the width of the cavity are likely to dictate the accessibility of the cavity to a ligand. The depth of the cavity, defined by the distance between the sulfur atom of Cys220 and the C_α of Pro222, also fluctuated within a range comparable to that observed in the crystal structures (Figure 4B). The cavity depth was altered significantly only when isopropanol was within the cavity, suggesting an induced-fit phenomenon. At present, whether the induced-fit movements of the cysteine upon ligand binding have an associated energetic penalty remains unclear. In this context, it is interesting to note that this cysteine flip was not observed upon binding of PhiKan083 (Boeckler et al., 2008).

Mutations that lead to increased atomic fluctuations have been linked to the instability of proteins (Interlandi et al., 2008). Our structural and MD observations reveal the cavity region of p53-Y220C to be highly dynamic. To determine whether binding of the fragments alters the plasticity of the cavity, we investigated the dynamics of T-p53C-Y220C in complex with the fragments using Gaussian network model (GNM) analysis (Yang et al., 2006). The GNM represents the protein as an elastic network where harmonic springs connect neighboring nodes (distance <10 Å) centered on the C_α-atoms of residues in the native structure. The GNM has been shown to be highly accurate in reproducing experimental data on structural fluctuations of biological macromolecules (i.e., crystallographic B-factors and H/D exchange protection factors) (Bahar et al., 1997; Bahar

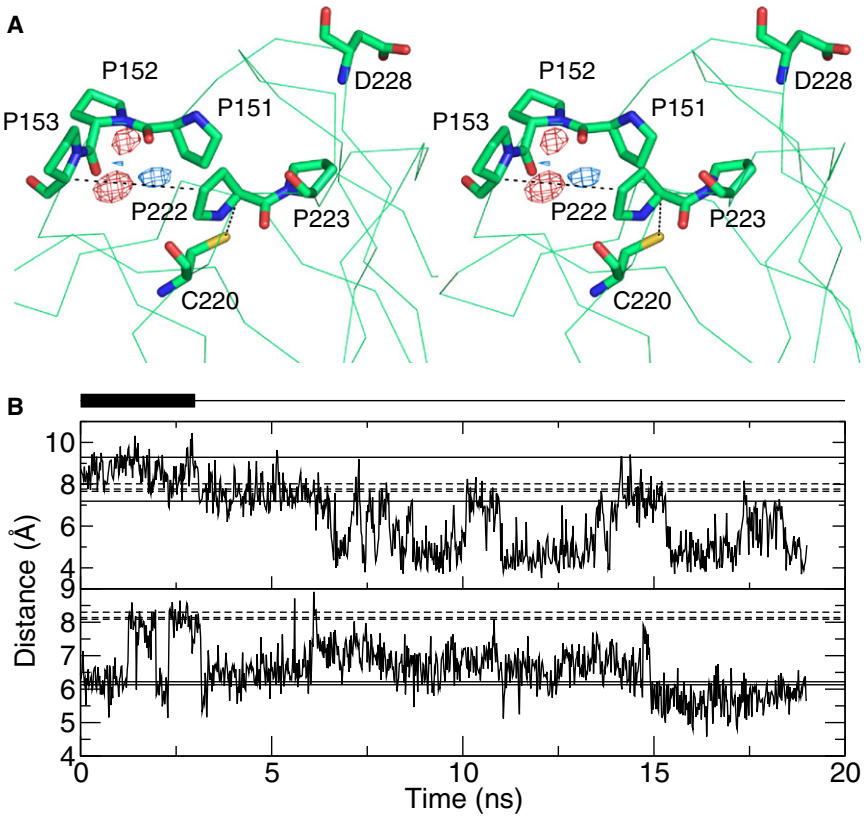

Figure 4. Preferential Solvation of the Surface of T-p53C-Y220C with Isopropanol

(A) The density of isopropanol oxygen (red) and carbon (blue) atoms in the cavity contoured at four times the density of the bulk mixture. The view is similar to that of the fragment complexes in Figure 3.

(B) Distance between the C_α atom of Pro153 and the C_γ atom of Pro222 (top plot), and between the C_α atom of Pro222 and sulfur atom of Cys220 (bottom plot), as a function of time. The solid line represents the distance between the same atoms in the crystal structure of free T-p53C-Y220C (PDB code 2J1X chains A and B). The dashed lines represent the distances between the same atoms in the fragment-bound structures.

et al., 1998) and has been widely used to study the functional consequence of those fluctuations (Bahar et al., 1999; Tobi and Bahar, 2005). In the context of the GNM, the presence of the fragments in the mutational cavity is introduced by extending the model's elastic network to include select atoms of the fragments. Protein-fragment interactions are therefore assigned with the same nonspecific character as protein-protein interactions. Accordingly, such interactions are dependent only on the size and position of the fragments within the pocket and do not account for the chemical nature of the fragments.

Results of the GNM analysis (Figure 5) found that the presence of the fragments markedly reduces the flexibility of the cavity region. The backbone dynamics of T-p53C-Y220C in the cavity upon binding of the fragments are virtually identical to that of wild-type p53 core domain. The fragments presumably couple the proline-rich loops that line the mutational cavity to the rest of the protein, thus enhancing the rigidity of the region. The loops in T-p53C-Y220C in the absence of fragments are, instead, loose and very flexible, highlighting the importance of the tyrosine ring system in the wild-type protein in holding the proline-rich loops together, thereby stabilizing the local structure. This result is supported by the observation that Pro222 exhibits significantly reduced temperature factors in the crystal structures of all Y220C-ligand complexes compared with the structure of the ligand-free mutant.

Implications for Rescue of p53-Y220C

The binding sites of the fragments partly overlap with that of PhiKan083 (Figure 6). In the Y220C-PhiKan083 complex, the N-ethyl substituent of the central carbazole ring system serves as a hydrophobic anchor, occupying the deepest part of the binding pocket, next to the sulfhydryl group of Cys220 (Boeckler et al., 2008). The cysteine flip observed upon binding of fragment 15 further extends the cavity depth as a result of the benzothiazole ring system sitting much deeper in the pocket than the carbazole ring system of PhiKan083 (Figure 6A). Consequently, Thr150 at the upper rim of the binding pocket sits closer to the center of the cavity compared with Phikan083. The fragments also address parts of the cavity, next to Pro153, that are not occupied by PhiKan083. On the other hand, the protonated methanamine moiety of PhiKan083 is hydrogen-bonded to the main-chain oxygen of Asp228, at a site of the cavity that is not occupied by the fragments.

The results of fragment screening and MD have considerable implications toward the rational design of lead ligands that stabilize p53-Y220C. When taken together, the collection of fragment-binding modes and preferential sites of isopropanol

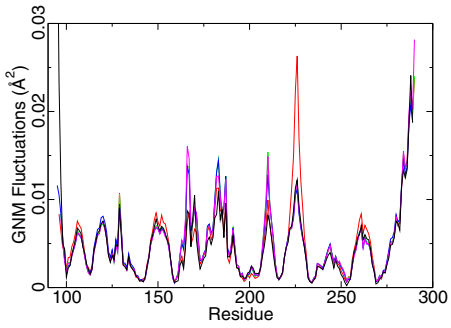

Figure 5. Distribution of the Slowest Global Fluctuations

Shown are the slowest global fluctuations (average of modes 1–3) of wild-type p53 (black line), free T-p53C-Y220C (red line) and T-p53C-Y220C bound to fragments 15 (green), 11 (blue) and 2 (magenta) determined by Gaussian network modeling. A 10 Å cutoff for amino acid pairs (C_α-C_α) was used in the analysis.

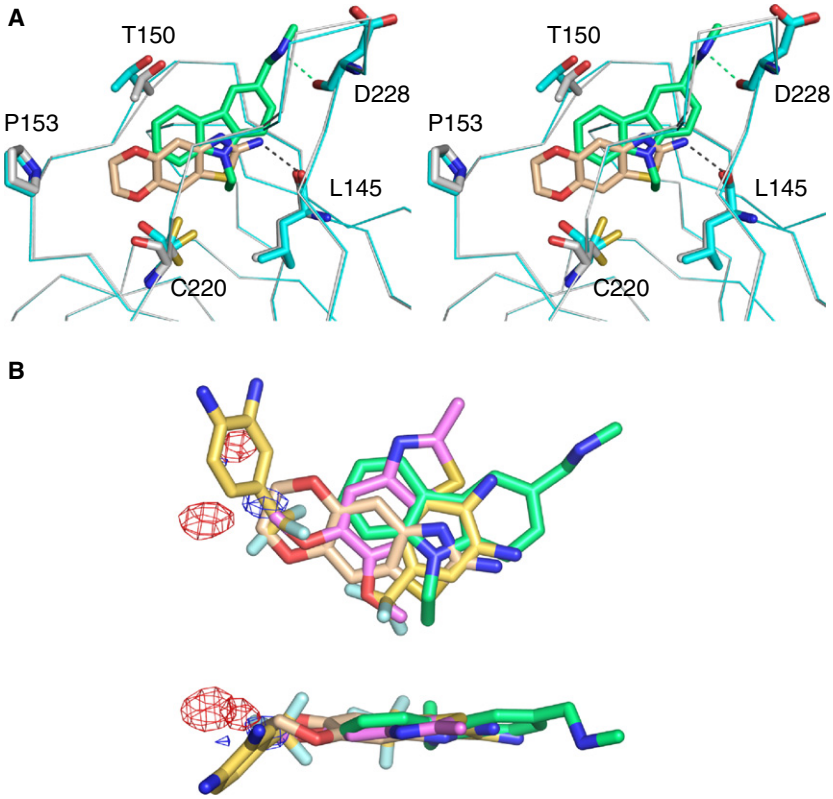

Figure 6. Overlay of Lead Fragment Hits

(A) Stereo view of the structure of T-p53C-Y220C (gray) in complex with the benzothiazole-based fragment 15 (beige) superimposed onto the structure of T-p53C-Y220C (cyan) bound to Phikan083 (green) (PDB code 2VUK) (Boeckler et al., 2008).

(B) Overlay of lead fragment hits from this study, Phikan083, and density of isopropanol oxygen (red) and carbon (blue) atoms in the cavity of T-p53C-Y220C from MD simulations contoured at four times the density of the bulk mixture. The superposition is based on the complete B chain of all structures. Protein atoms are omitted for clarity. The color code of the fragments is the same as in Figure 3 with PhiKan083 shown in green. Two views are shown: side view (upper panel) and view from the top of the cavity after 90° rotation around the *x*-axis (lower panel).

solvation provide a detailed map of ligand-binding sites in the mutational cavity. Importantly, the overlay of the fragments and isopropanol-binding sites fill the cavity completely, thereby revealing a multitude of interaction points on the cavity surface (Figure 6B). Using this information, the binding efficiency of the fragment hits can, in principle, be improved by either enlarging the constituent fragments to incorporate adjacent interaction sites or tethering fragments with complementary binding modes. The structure of T-p53C-Y220C with two molecules of fragment 2 bound at different sites illustrates nicely how fragments with different binding modes can be linked to encompass multiple interaction sites (Figure 3C). The binding free energy of an optimized ligand should be the sum of the energies of the individual subsites, enhanced by an entropy term (the "chelate effect") (Horovitz and Fersht, 1992) and negated by any unfavorable energetic penalties imposed by the linkers (Erlanson, 2006).

Our understanding of the structural plasticity of the cavity region can also aid in the design of lead ligands with improved binding affinities. Conformational changes in the cavity can significantly alter the cavity geometry and, in turn, the orientation of ligand interaction sites with respect to one another. Introducing flexible regions into the ligand increases the likelihood the ligand can adapt to the plasticity of the target binding site. The incorporation of flexibility in ligand design is reminiscent of the strategy used to circumvent mutation resistance that stems from changes in binding-site structure (Das et al., 2008; Teague, 2003). In addition, flexibility may be incorporated into computational approaches for ligand design.

SIGNIFICANCE

The tumor suppressor p53, a key protein in safeguarding cells from growing unchecked, is widely mutated in human cancers. Small molecules that bind to and rescue the function of mutant p53 thus have broad implications as anticancer therapeutics. The p53 cancer mutation Y220C, which destabilizes p53, presents a unique opportunity to target mutant p53. The mutation induces formation of a surface cavity that can accommodate stabilizing small molecules. Our results paint a clear picture of how a druglike molecule could dock within the mutational cavity of the Y220C mutant. Specifically, we have mapped ligand-binding sites in the mutational cavity of p53-Y220C using fragment screening and MD. The combination of fragment-based screening and MD simulation, as exemplified here, could, more broadly, be applied to map key interaction sites in novel targets. Structural elucidation of the binding modes of several of the fragments shows, with atomistic detail, the interactions responsible for stabilizing the fragment in the cavity region. Moreover, observation of the dynamic landscape of the cavity region highlight the relationship between protein flexibility and stability. The fragment hits, as shown by MD, markedly reduce the backbone dynamics of T-p53-Y220C in the cavity region, thus stabilizing the protein's local structure. Ultimately, these finding provide the framework for the rational design of lead ligands that rescue the transcriptional activity of the oncogenic p53-Y220C by selectively targeting the mutation site.

EXPERIMENTAL PROCEDURES

Fragment Library

Fragments were purchased from Chembridge (San Diego, CA), Life Chemicals (Kiev, Ukraine), and Maybridge (Cornwall, United Kingdom).

Protein Expression and Purification

The T-p53-Y220C protein, containing p53 residues 94–312, was produced following the procedure described for wild-type p53 (Boeckler et al., 2008).

The protein contained an N-terminal His6 lipoyl tag that was cleaved after purification. For $^{15}N/^{1}H$ HSQC experiments, the protein was expressed in M9 minimal media with $^{15}NH_4Cl$ as the only nitrogen source. For crystallization, a tag-free form of the protein was produced and purified.

Fragment Screening by Thermal Denaturation Scanning Fluorimetry

The effect of ligands on the T_m of T-p53C-Y220C was monitored via high-resolution melt analysis using a Corbett (Mortlake, Australia) Rotor-Gene 6000 real-time PCR thermocycler. Briefly, the protein (15 μM) was mixed with the fluorescent dye SYPRO orange (Invitrogen, CA; diluted 1000-fold) in buffer (25 mM potassium phosphate, 150 mM NaCl, and 5 mM DTT [pH 7.5]) with 1 mM fragment, which was added from 20 mM stock solutions in neat DMSO (5% v/v final concentration). Fluorescence of the dye was measured continuously while ramping the temperature from 30 to 50°C at a rate of 0.1°C/s using excitation and emission filters of 460 and 510 nm, respectively. The T_m of the protein with the addition of fragment was determined from the derivative of the fluorescence versus temperature curve and was compared to control samples consisting of protein with DMSO only. All samples were measured in triplicate. Fragments that raised the T_m of the protein by 0.5°C or greater were considered hits.

Fragment Screening by WaterLOGSY

WaterLOGSY experiments were performed at 20°C on a Bruker DRX500 spectrometer (500 MHz ^{1}H frequency) equipped with a 5-mm inverse cryogenic probe head. Fragments were screened in mixtures of five, at an individual concentration of 300 μM in 25 mM sodium phosphate and 150 mM NaCl (pH 7.2) with 5% v/v DMSO-d_6. Ligand binding was identified by the decrease or reversal in intensity of the ligand signal in the presence of protein. Because the ligand mixtures were designed to avoid resonance overlap between the difference components, additional deconvolution of mixtures of hits was not necessary. All spectra were recorded with an NOE mixing time of 900 ms and a recycle delay of 2.5 s. For each individual spectrum, 128 transients were acquired with 4096 time domain data points, covering a spectral width of 6.0 kHz (centered on resonance for water).

$^{15}N/^{1}H$ HSQC Analysis of Fragment Binding

$^{15}N/^{1}H$ HSQC spectra of T-p53-Y220C (75 μM) were acquired at 20°C on a Bruker Avance-800 spectrometer (800 MHz ^{1}H frequency) using a 5-mm inverse cryogenic probe. Samples were prepared by adding ligand (1 mM) to buffer (25 mM sodium phosphate, 150 mM NaCl, and 5 mM DTT [pH 7.2]) with 5% (v/v) DMSO-*d6*. Using the criteria for hit identification defined by Hajduk et al. (1997), the minimum threshold for significant perturbations in ^{15}N or ^{1}H nuclei was 0.1 ppm.

Crystallographic Determination of Fragment-Binding Mode

Crystals of T-p53C-Y220C were grown via the sitting drop vapor diffusion method, as described elsewhere (Joerger et al., 2006). They were soaked in solutions of fragment (100 mM or saturated solution) in cryo buffer (19% w/v polyethylene glycol 4000, 20% v/v glycerol, 10 mM sodium phosphate [pH 7.2], 100 mM HEPES [pH 7.2], 150 mM KCl, and 10 mM DTT) for a minimum of 6 hr and flash frozen in liquid nitrogen. X-ray data sets were collected at 100 K at the Diamond Lights Source, Oxford (beamline I02), and the ESRF, Grenoble (beamlines ID14-1 and ID14-2). All data sets were processed with MOSFLM (Leslie, 1999) and SCALA (Evans, 2006). The structure was solved by rigid body refinement with PHENIX (Adams et al., 2002) using the structure of the ligand-free mutant (PDB ID 2J1X) as starting model. After an initial round of refinement, water molecules were added to the structures using PHENIX. The fragments were then manually built into the structure using MAIN (Turk, 1992), and the resulting models were further refined with PHENIX. Data collection and refinement statistics are shown in Table 2.

MD Simulations

Simulations of the T-p53-Y220C mutant (PDB ID 2VUK chain A), explicitly solvated in a mixture of isopropanol (20% v/v) and water, were computed using the CHARMM (Brooks et al., 1983) and NAMD (Phillips et al., 2005) programs and the param22 all-atom force field (MacKerell et al., 1998) for a productive trajectory of 19 ns. Details of the simulation protocol are reported in the Supplemental Information.

Analysis of the trajectories was performed using WORDOM (Seeber et al., 2007), VMD (Humphrey et al., 1996), and the GROMACS analysis tools (Hess et al., 2008). The procedure for determining solvation and druggability was described previously by Seco et al. (2009) and is summarized in the Supplemental Information.

ACCESSION NUMBERS

Coordinates and structure factors have been deposited in the Protein Data Bank (www.pdb.org) under PDB ID codes 2X0U, 2X0V, and 2X0W.

SUPPLEMENTAL INFORMATION

Supplemental Information includes two figures and Supplemental Experimental Procedures and can be found with this article online at doi:10.1016/j.chembiol.2009.12.011.

ACKNOWLEDGMENTS

This work was supported by the Medical Research Council and EU FP6 funding. We thank Caroline Blair for assistance with protein production, Jeremy Touati and Stephan Hammer for help preparing of protein crystals, Mark Allen for technical advice on crystallography, and the staffs at beamlines ID14-1 and ID14-2 at the European Synchrotron Radiation Facility (Grenoble, France) and at beamline I02 at the Diamond Light Source (Didcot, UK) for support with crystallographic data collection. We are also grateful to Chris Johnson for insightful comments on fragment optimization. N.B. and J.L.K. are supported by Medical Research Council Career Development Fellowships.

Received: August 4, 2009
Revised: November 27, 2009
Accepted: December 14, 2009
Published: January 28, 2010

REFERENCES

Adams, P.D., Grosse-Kunstleve, R.W., Hung, L.W., Ioerger, T.R., McCoy, A.J., Moriarty, N.W., Read, R.J., Sacchettini, J.C., Sauter, N.K., and Terwilliger, T.C. (2002). PHENIX: building new software for automated crystallographic structure determination. Acta Crystallogr. D Biol. Crystallogr. *58*, 1948–1954.

Bahar, I., Atilgan, A.R., and Erman, B. (1997). Direct evaluation of thermal fluctuations in proteins using a single-parameter harmonic potential. Fold. Des. *2*, 173–181.

Bahar, I., Wallqvist, A., Covell, D.G., and Jernigan, R.L. (1998). Correlation between native-state hydrogen exchange and cooperative residue fluctuations from a simple model. Biochemistry *37*, 1067–1075.

Bahar, I., Erman, B., Jernigan, R.L., Atilgan, A.R., and Covell, D.G. (1999). Collective motions in HIV-1 reverse transcriptase: examination of flexibility and enzyme function. J. Mol. Biol. *285*, 1023–1037.

Bembenek, S.D., Tounge, B.A., and Reynolds, C.H. (2009). Ligand efficiency and fragment-based drug discovery. Drug Discov. Today *14*, 278–283.

Boeckler, F.M., Joerger, A.C., Jaggi, G., Rutherford, T.J., Veprintsev, D.B., and Fersht, A.R. (2008). Targeted rescue of a destabilized mutant of p53 by an in silico screened drug. Proc. Natl. Acad. Sci. USA *105*, 10360–10365.

Bohm, H.J., Banner, D., Bendels, S., Kansy, M., Kuhn, B., Muller, K., Obst-Sander, U., and Stahl, M. (2004). Fluorine in medicinal chemistry. ChemBioChem *5*, 637–643.

Brooks, B.R., Bruccoleri, R.E., Olafson, B.D., States, D.J., Swaminathan, S., and Karplus, M. (1983). Charmm—a program for macromolecular energy, minimization, and dynamics calculations. J. Comput. Chem. *4*, 187–217.

Bullock, A.N., and Fersht, A.R. (2001). Rescuing the function of mutant p53. Nat. Rev. Cancer *1*, 68–76.

Bullock, A.N., Henckel, J., DeDecker, B.S., Johnson, C.M., Nikolova, P.V., Proctor, M.R., Lane, D.P., and Fersht, A.R. (1997). Thermodynamic stability of wild-type and mutant p53 core domain. Proc. Natl. Acad. Sci. USA *94*, 14338–14342.

Bullock, A.N., Henckel, J., and Fersht, A.R. (2000). Quantitative analysis of residual folding and DNA binding in mutant p53 core domain: definition of mutant states for rescue in cancer therapy. Oncogene *19*, 1245–1256.

Bykov, V.J., Issaeva, N., Shilov, A., Hultcrantz, M., Pugacheva, E., Chumakov, P., Bergman, J., Wiman, K.G., and Selivanova, G. (2002). Restoration of the tumor suppressor function to mutant p53 by a low-molecular-weight compound. Nat. Med. *8*, 282–288.

Bykov, V.J., Issaeva, N., Zache, N., Shilov, A., Hultcrantz, M., Bergman, J., Selivanova, G., and Wiman, K.G. (2005). Reactivation of mutant p53 and induction of apoptosis in human tumor cells by maleimide analogs. J. Biol. Chem. *280*, 30384–30391.

Ciulli, A., and Abell, C. (2007). Fragment-based approaches to enzyme inhibition. Curr. Opin. Biotechnol. *18*, 489–496.

Congreve, M., Carr, R., Murray, C., and Jhoti, H. (2003). A rule of three for fragment-based lead discovery? Drug Discov. Today *8*, 876–877.

Das, K., Bauman, J.D., Clark, A.D., Jr., Frenkel, Y.V., Lewi, P.J., Shatkin, A.J., Hughes, S.H., and Arnold, E. (2008). High-resolution structures of HIV-1 reverse transcriptase/TMC278 complexes: strategic flexibility explains potency against resistance mutations. Proc. Natl. Acad. Sci. USA *105*, 1466–1471.

Davis, I.W., Leaver-Fay, A., Chen, V.B., Block, J.N., Kapral, G.J., Wang, X., Murray, L.W., Arendall, W.B., 3rd, Snoeyink, J., Richardson, J.S., and Richardson, D.C. (2007). MolProbity: all-atom contacts and structure validation for proteins and nucleic acids. Nucleic Acids Res. *35*, W375–383.

Dennis, S., Kortvelyesi, T., and Vajda, S. (2002). Computational mapping identifies the binding sites of organic solvents on proteins. Proc. Natl. Acad. Sci. USA *99*, 4290–4295.

Di Como, C.J., and Prives, C. (1998). Human tumor-derived p53 proteins exhibit binding site selectivity and temperature sensitivity for transactivation in a yeast-based assay. Oncogene *16*, 2527–2539.

Erlanson, D.A. (2006). Fragment-based lead discovery: a chemical update. Curr. Opin. Biotechnol. *17*, 643–652.

Evans, P. (2006). Scaling and assessment of data quality. Acta Crystallogr. D Biol. Crystallogr. *62*, 72–82.

Foster, B.A., Coffey, H.A., Morin, M.J., and Rastinejad, F. (1999). Pharmacological rescue of mutant p53 conformation and function. Science *286*, 2507–2510.

Friedler, A., Hansson, L.O., Veprintsev, D.B., Freund, S.M., Rippin, T.M., Nikolova, P.V., Proctor, M.R., Rudiger, S., and Fersht, A.R. (2002). A peptide that binds and stabilizes p53 core domain: chaperone strategy for rescue of oncogenic mutants. Proc. Natl. Acad. Sci. USA *99*, 937–942.

Friedler, A., Veprintsev, D.B., Hansson, L.O., and Fersht, A.R. (2003). Kinetic instability of p53 core domain mutants: implications for rescue by small molecules. J. Biol. Chem. *278*, 24108–24112.

Guvench, O., and MacKerell, A.D., Jr. (2009). Computational fragment-based binding site identification by ligand competitive saturation. PLoS Comput. Biol. *5*, e1000435.

Hajduk, P.J., and Greer, J. (2007). A decade of fragment-based drug design: strategic advances and lessons learned. Nat. Rev. Drug Discov. *6*, 211–219.

Hajduk, P.J., Dinges, J., Miknis, G.F., Merlock, M., Middleton, T., Kempf, D.J., Egan, D.A., Walter, K.A., Robins, T.S., Shuker, S.B., et al. (1997). NMR-based discovery of lead inhibitors that block DNA binding of the human papillomavirus E2 protein. J. Med. Chem. *40*, 3144–3150.

Hajduk, P.J., Huth, J.R., and Fesik, S.W. (2005a). Druggability indices for protein targets derived from NMR-based screening data. J. Med. Chem. *48*, 2518–2525.

Hajduk, P.J., Huth, J.R., and Tse, C. (2005b). Predicting protein druggability. Drug Discov. Today *10*, 1675–1682.

Hann, B.C., and Lane, D.P. (1995). The dominating effect of mutant p53. Nat. Genet. *9*, 221–222.

Hess, B., Kutzner, C., van der Spoel, D., and Lindahl, E. (2008). GROMACS 4: Algorithms for highly efficient, load-balanced, and scalable molecular simulation. J. Chem. Theory Comput. *4*, 435–447.

Hollstein, M., Sidransky, D., Vogelstein, B., and Harris, C.C. (1991). p53 mutations in human cancers. Science *253*, 49–53.

Horovitz, A., and Fersht, A.R. (1992). Co-operative interactions during protein folding. J. Mol. Biol. *224*, 733–740.

Humphrey, W., Dalke, A., and Schulten, K. (1996). VMD: Visual molecular dynamics. J. Mol. Graph. *14*, 33–38.

Interlandi, G., Wetzel, S.K., Settanni, G., Pluckthun, A., and Caflisch, A. (2008). Characterization and further stabilization of designed ankyrin repeat proteins by combining molecular dynamics simulations and experiments. J. Mol. Biol. *375*, 837–854.

Issaeva, N., Friedler, A., Bozko, P., Wiman, K.G., Fersht, A.R., and Selivanova, G. (2003). Rescue of mutants of the tumor suppressor p53 in cancer cells by a designed peptide. Proc. Natl. Acad. Sci. USA *100*, 13303–13307.

Joerger, A.C., and Fersht, A.R. (2007). Structure-function-rescue: the diverse nature of common p53 cancer mutants. Oncogene *26*, 2226–2242.

Joerger, A.C., and Fersht, A.R. (2008). Structural biology of the tumor suppressor p53. Annu. Rev. Biochem. *77*, 557–582.

Joerger, A.C., Allen, M.D., and Fersht, A.R. (2004). Crystal structure of a superstable mutant of human p53 core domain. Insights into the mechanism of rescuing oncogenic mutations. J. Biol. Chem. *279*, 1291–1296.

Joerger, A.C., Ang, H.C., and Fersht, A.R. (2006). Structural basis for understanding oncogenic p53 mutations and designing rescue drugs. Proc. Natl. Acad. Sci. USA *103*, 15056–15061.

Kitayner, M., Rozenberg, H., Kessler, N., Rabinovich, D., Shaulov, L., Haran, T.E., and Shakked, Z. (2006). Structural basis of DNA recognition by p53 tetramers. Mol. Cell *22*, 741–753.

Lambert, J.M., Gorzov, P., Veprintsev, D.B., Soderqvist, M., Segerback, D., Bergman, J., Fersht, A.R., Hainaut, P., Wiman, K.G., and Bykov, V.J. (2009). PRIMA-1 reactivates mutant p53 by covalent binding to the core domain. Cancer Cell *15*, 376–388.

Leslie, A.G. (1999). Integration of macromolecular diffraction data. Acta Crystallogr. D Biol. Crystallogr. *55*, 1696–1702.

Levine, A.J., Momand, J., and Finlay, C.A. (1991). The p53 tumour suppressor gene. Nature *351*, 453–456.

Liepinsh, E., and Otting, G. (1997). Organic solvents identify specific ligand binding sites on protein surfaces. Nat. Biotechnol. *15*, 264–268.

MacKerell, A.D., Bashford, D., Bellott, M., Dunbrack, R.L., Evanseck, J.D., Field, M.J., Fischer, S., Gao, J., Guo, H., Ha, S., et al. (1998). All-atom empirical potential for molecular modeling and dynamics studies of proteins. J. Phys. Chem. B *102*, 3586–3616.

Meyer, B., and Peters, T. (2003). NMR spectroscopy techniques for screening and identifying ligand binding to protein receptors. Angew. Chem. Int. Ed. Engl. *42*, 864–890.

Nikolova, P.V., Henckel, J., Lane, D.P., and Fersht, A.R. (1998). Semirational design of active tumor suppressor p53 DNA binding domain with enhanced stability. Proc. Natl. Acad. Sci. USA *95*, 14675–14680.

North, S., Pluquet, O., Maurici, D., El-Ghissassi, F., and Hainaut, P. (2002). Restoration of wild-type conformation and activity of a temperature-sensitive mutant of p53 (p53(V272M)) by the cytoprotective aminothiol WR1065 in the esophageal cancer cell line TE-1. Mol. Carcinog. *33*, 181–188.

Petitjean, A., Mathe, E., Kato, S., Ishioka, C., Tavtigian, S.V., Hainaut, P., and Olivier, M. (2007). Impact of mutant p53 functional properties on TP53 mutation patterns and tumor phenotype: lessons from recent developments in the IARC TP53 database. Hum. Mutat. *28*, 622–629.

Phillips, J.C., Braun, R., Wang, W., Gumbart, J., Tajkhorshid, E., Villa, E., Chipot, C., Skeel, R.D., Kale, L., and Schulten, K. (2005). Scalable molecular dynamics with NAMD. J. Comput. Chem. *26*, 1781–1802.

Seco, J., Luque, F.J., and Barril, X. (2009). Binding site detection and druggability index from first principles. J. Med. Chem. *52*, 2363–2371.

Seeber, M., Cecchini, M., Rao, F., Settanni, G., and Caflisch, A. (2007). Wordom: a program for efficient analysis of molecular dynamics simulations. Bioinformatics *23*, 2625–2627.

Teague, S.J. (2003). Implications of protein flexibility for drug discovery. Nat. Rev. Drug Discov. *2*, 527–541.

Tobi, D., and Bahar, I. (2005). Structural changes involved in protein binding correlate with intrinsic motions of proteins in the unbound state. Proc. Natl. Acad. Sci. USA *102*, 18908–18913.

Turk, D. (1992). PhD thesis. Technische Universität München, Munich, Germany.

Vousden, K.H., and Lane, D.P. (2007). p53 in health and disease. Nat. Rev. Mol. Cell Biol. *8*, 275–283.

Yang, L.W., Rader, A.J., Liu, X., Jursa, C.J., Chen, S.C., Karimi, H.A., and Bahar, I. (2006). oGNM: online computation of structural dynamics using the Gaussian Network Model. Nucleic Acids Res. *34*, W24–31.

